Fourth International Symposium on Marine Propulsors
smp'15, Austin, Texas, USA, June 2015

A Calculation Method Based on QCM for Characteristics of Propeller with Energy Saving Duct in Steady Ship's Wake

Koichiro Shiraishi[1], Koichi Koyama[1], Hikaru Kamiirisa[1]

[1] Fluid Control Research Group, Fluids Engineering and Hull Design Department, National Maritime Research Institute, Japan

ABSTRACT

This paper presents a calculation method for characteristics of propeller with energy saving duct in steady ship's wake. The method is based on a QCM (**Q**uasi-**C**ontinuous vortex lattice **M**ethod). The QCM method has been highly appraised in this field, because of its simplicity, and especially of its reasonableness in obtaining proper solution for various types of propellers.

In this paper, authors describe how to apply QCM to the calculation for characteristics of propellers with energy saving duct and show some calculated results in steady ship's wake. The authors also studied on the mechanism of interaction between the propeller and the energy saving duct.

Keywords

Propeller Performance, Energy Saving Ducts, Ship's Wake, Quasi-Continuous Method, Unsteady Calculation

1 INTRODUCTION

With increased attention of international movement against global warming, the energy saving is required in shipbuilding industry. The various energy saving devices have been developed. It is important to estimate the performance of ship equipped with these devices in ship design. However, the location and shape of device is different in every type of ship, and to determine the optimal location and shape with experiment is difficult due to the scale effect.

In this study, the authors have developed a new calculation method using QCM for characteristics of propeller with energy saving duct in steady ship's wake. This duct is a stern duct type energy saving device. Figure 1 shows the target energy saving duct in this study.

QCM is a numerical method for the lifting surface theory, which was developed by Lan (1974) originally to solve planar wing problems. Since its development, it has been successfully applied to estimation of the thrust and torque of various propellers in a uniform and non-uniform inflow (Hoshino, 1985 and Nakamura, 1985). Hanaoka (2014) evaluated the performance of propellers with energy saving ducts in uniform flow. However, in ship design, it is important to evaluate the performance of those propellers in the ship's wake.

Therefore, the authors have developed an unsteady calculation method for evaluating the propellers with energy saving dust in non-uniform flow. In this calculation, a hydrodynamic pitch which is determined by a rigorous lifting line theory is introduced for a trailing vortex model of propeller.

The authors present calculation results using developed method to the propeller with various energy saving ducts in ship's wake. Furthermore, the authors also have studied on the mechanism of interaction between the propeller and the energy saving ducts.

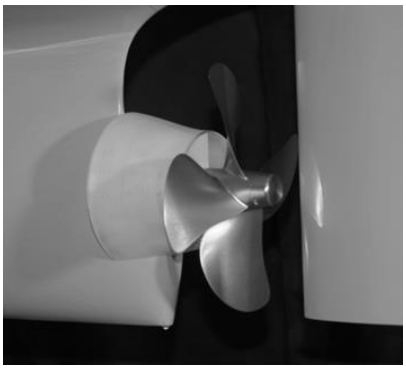

Figure 1: Photo of model ship installed propeller with energy saving duct (Kawashima, 2014).

2 COORDINATES SYSTEMS FOR PROPELLER WITH ENERGY SAVING DUCT

In QCM, discrete vortex distributions are arranged on the mean camber surface based on the semi-circle method (Lan 1974). These singularities should satisfy the boundary condition that the normal velocity is zero on the mean camber surfaces.

Consider a propeller rotating with a constant angular speed Ω ($= 2\pi n$, n is a number of propeller revolutions.). The direction of the rotation is counter-clockwise in the view of Fig. 2. The propeller operates in a non-uniform flow with the velocity $\mathbf{v}_0 = (v_{x0}, v_{y0}, v_{z0})$ of an unbound, incompressible, and inviscid fluid. The propeller consists of

K-blades which have the same shape and are placed symmetrically around the axis of the rotation.

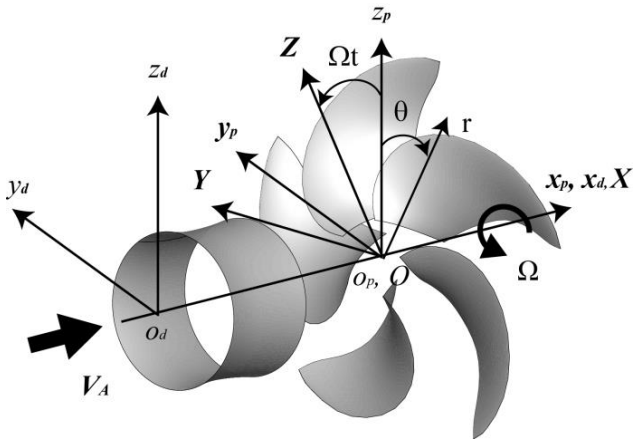

Figure 2: Coordinate Systems of propeller with energy saving duct.

As shown in Fig. 2, the space coordinate system □ − □□□ , the propeller coordinate system □□ − □□□□□ , and the duct coordinate system □□ − □□□□□ are introduced. Note that the subscript □ and □ denote the propeller and the duct, respectively. The cylindrical coordinate system □□ − □□□□□ and □□ − □□□□□ are also introduced for convenience. The angular coordinate □□ and □□ is measured clockwise from the z-axis when viewed in the direction of positive □. Then, the cylindrical coordinate system □ − □□□ can be transformed into the Cartesian coordinate system □ − □□□ as

$$□ = □, □ = −□\sin□, □ = □\cos□ \quad (1)$$

Where $□ = \sqrt{□^2 + □^2}, □ = \tan^{-1}(−□/□)$

The above equation is completed in the propeller and duct coordinates.

The propeller is rotating clockwise around the X-axis when looking forward. Then the space coordinate system □ − □□□ is transformed into the propeller coordinate system □□ − □□□□□ at any instant □ by the relations

$$□ = □□ \quad (2)$$

$$□ = □□\cos(Ω□) + □□\sin(Ω□) \quad (3)$$

$$□ = −□□\sin(Ω□) + □□\cos(Ω□) \quad (4)$$

as shown in Fig.2.

Fig. 3 shows the geometry of the energy saving duct, in which □□ represents the diameter of the duct. The duct geometry has a uniform shape of a cross section. Then, the duct coordinate system □□ − □□□□□ can be transformed into the space coordinate system □ − □□□ as

$$□ = □□ − □□ \quad (5)$$

$$□ = □□ \quad (6)$$

$$□ = □□ \quad (7)$$

Where □□ is the distance between center of propeller and the leading edge of the duct □□ is an attack angle of the duct and □□ is the chord length of the duct.

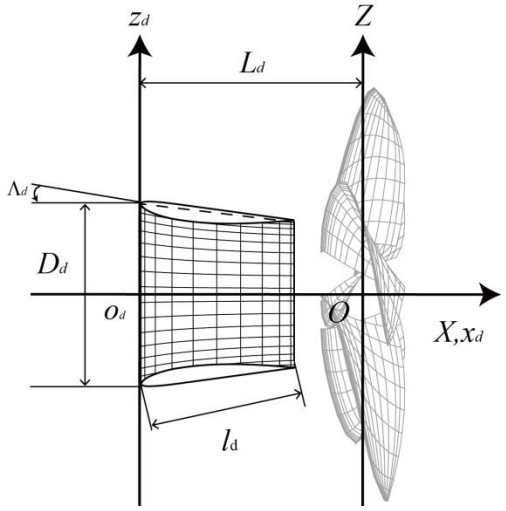

Figure 3: Geometry and coordinate of the energy saving duct.

3 NUMERICAL METHOD BASED ON QCM

3.1 Numerical Models of Propeller

The propeller blades and the duct profile are assumed to be thin. The hubs and shafts of the propellers are neglected. The propeller blades and the duct are represented by the distribution of bound vortices on the mean camber surfaces. The bound vortex distribution represents the load acting on the surfaces. According to Kelvin's theorem of vorticity conservation, the free vortices shed downstream from the bound vortices. Due to the shedding free vortices, horseshoe vortices are generated on the mean camber surfaces.

In this calculation method, the positions of loading point and control point are determined Kanemaru's method (2009). The mean camber surface is divided into □□ segments in the spanwise direction and divided into □□ in the chordwise direction. Here we introduce □ axis whose origin locates at the leading edge and is extended to the trailing vortex surface along the mean camber surface. The radial coordinates *r* of the loading and control points on the propeller blades are defined as

$$\square_{\square,\square} = \frac{1}{2}(\square_{\square,0} + \square_{\square,h}) - \frac{1}{2}(\square_{\square,0} - \square_{\square,h})\cos\square_{\square,\square} \quad (8)$$

$$\square_{\square,\square} = \frac{1}{2}(\square_{\square,\square} + \square_{\square,\square+1}) \quad (9)$$

$$\square_{\square,\square} = \frac{2\square - 1}{2(\square_{\square} + 1)}\square, \square = 1,2,\cdots,\square_{\square} + 1 \quad (10)$$

Where $\square_{\square,0}$ and $\square_{\square,h}$ are the radius of the propeller and the hub, respectively. The position of the bound vortex $\square^{\square\square}_{\square,\square\square}$ and control point $\square^{\square\square}_{\square,\square\square}$ on the mean camber surface are expressed by the following equations.

$$\square^{\square\square}_{\square,\square\square} = \square_{\square,\square}(\square_{\square,\square}) + \frac{\square_{\square,\square}(\square_{\square,\square}) - \square_{\square,\square}(\square_{\square,\square})}{2}(1 - \cos\frac{2\square - 1}{2\square_{\square}}\square) \quad (11)$$

$$\square^{\square\square}_{\square,\square\square} = \square_{\square,\square}(\overline{\square_{\square,\square}}) + \frac{\square_{\square,\square}(\overline{\square_{\square}}) - \square_{\square,\square}(\overline{\square_{\square+1}})}{2}(1 - \cos\frac{\square}{\square_{\square}}\square) \quad (12)$$

3.2 Numerical Models of Duct

In same ways of the propeller, the mean camber surface of duct is divided into $\square_{\square}$ segments in the circumferential direction and divided into $\square_{\square}$ in the chordwise direction. The position of the bound vortex $\square^{\square\square}_{\square,\square\square}$ and control point $\square^{\square\square}_{\square,\square\square}$on the duct mean camber surface are expressed by the following equations.

$$\square^{\square\square}_{\square,\square\square} = \square_{\square}\cos\Lambda\left(1 - \cos\frac{2\square - 1}{2\square_{\square}}\square\right) \quad (13)$$

$$\square^{\square\square}_{\square,\square\square} = \square_{\square}\cos\Lambda\left(1 - \cos\frac{\square}{\square_{\square}}\square\right) \quad (14)$$

$$\square^{\square\square}_{\square,\square\square} = (1 - \square_{\square}\sin\Lambda)\sin\left(\frac{2\square - 1}{2(\square_{\square} + 1)}\square\right) \quad (15)$$

$$\square^{\square\square}_{\square,\square\square} = (1 - \square_{\square}\sin\Lambda)\sin\left(\frac{\square}{\square_{\square} + 1}\square\right) \quad (16)$$

$$\square^{\square\square}_{\square,\square\square} = (1 - \square_{\square}\sin\Lambda)\cos\left(\frac{2\square - 1}{2(\square_{\square} + 1)}\square\right) \quad (17)$$

$$\square^{\square\square}_{\square,\square\square} = (1 - \square_{\square}\sin\Lambda)\cos\left(\frac{\square}{\square_{\square} + 1}\square\right) \quad (18)$$

3.3 Numerical Models of Trailing Vortex

The free vortices shed from the bound vortices are considered to leave from the trailing edge and flow into the slipstream with the local velocity at the position. In this method, a hydrodynamic pitch which is determined by a rigorous lifting line theory is introduced for a trailing vortex model of propeller. This trailing vortex model has been used by Hanaoka (1969) and Koyama (1975). The effectiveness has been shown in their research. The hydrodynamic pitch is expressed by the following equation

$$h(\square) = \frac{\square + \overline{\square_{\square}}}{\Omega + \overline{\square_{\square}}/\square} \quad (19)$$

Where $\square$ is a propeller advance velocity, $\overline{\square_{\square}}$ is an averaged induced velocity in the x-axial component and $\overline{\square_{\square}}$ is an averaged induced velocity in tangential component. Fig. 4 shows the shapes of the trailing vortex sheets used in the present calculations.

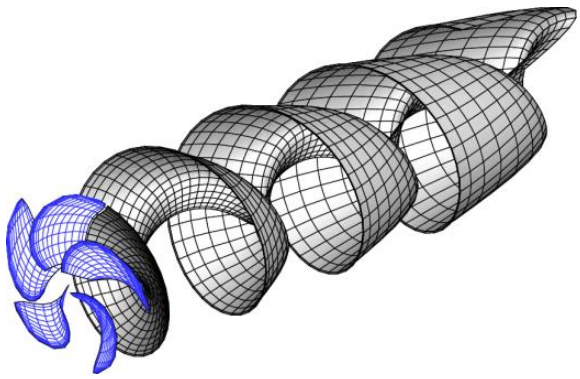

Figure 4: Perspective views of the trailing vortex sheets leaving from the first propeller blade.

For the duct, the trailing vortex sheet leaves the trailing edge of the duct and remains straight along the $\square$-axis. Thus, the duct trailing vortex is cylindrical with $\square$-axis as the center line. This model for the trailing vortex is same as that used in Yuasa (1980). Fig. 5 shows the shapes of the trailing vortex sheets used in this calculation.

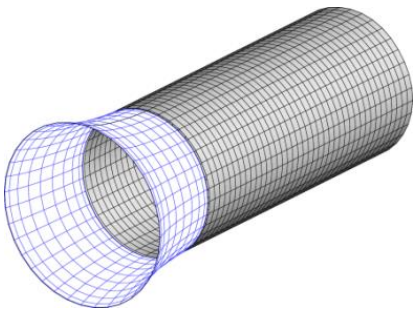

Figure 5: Perspective views of the trailing vortex sheets leaving from energy saving duct.

The vortices are assumed to be shed from the trailing edge with uniform spatial interval. Fig.6 shows the illustration of the shed vortices in case of the propeller and duct.

3.4 Calculation of Induced Velocity

These induced velocity vector are expressed as

$$\square^{\square}_{\square\square\square} = \square^{\square}_{\square\square\square} + \sum_{\square=\square}^{\square_{\square}} \left(\square^{\square}_{\square\square+\square\square'} - \square^{\square}_{\square\square\square'}\right) - \square^{\square\square}_{\square\square\square}\, l_{\square=\square} \tag{20}$$

$$\square^{\square}_{\square\square\square} = \square^{\square\square}_{\square\square\square} - \square^{\square\square}_{\square\square\square+\square} + \square^{\square\square}_{\square\square+\square\square} - \square^{\square\square}_{\square\square\square} \tag{21}$$

Where

$\square^{\square}_{\square\square\square}$ = induced velocity vector due to the bound vortex of unit strength on the mean camber surface

$\square^{\square}_{\square\square\square}$ = induced velocity vector due to the free vortex of unit strength on the mean camber surface

$\square^{\square\square}_{\square\square\square}$ = induced velocity vector due to the spanwise shed vortex of unit strength in the trailing wake

$\square^{\square\square}_{\square\square\square}$ = induced velocity vector due to the streamwise trailing vortex of unit strength in the trailing wake

The induced velocity vector $\square$ due to each line segment of vortex is calculated by the Biot-Savart law.

(a) Propeller

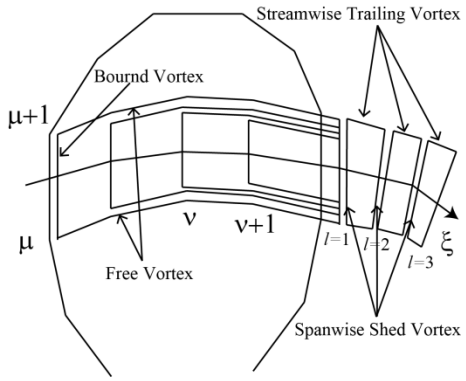

(b) Energy saving duct

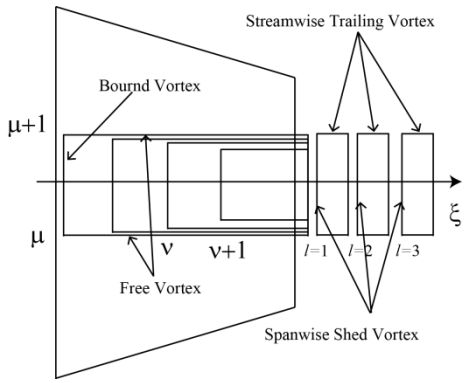

Figure 6: Arrangement of vortex system

If we define the segments of the ring vortex on the mean camber surface at time $\square_{\square}$ and the ring vortex in the trailing wake as $\square_{\square\square\square}(\square_{\square})$ and $\Gamma_{\square\square\square}(\square_{\square})$, the induced velocity vector due to the vortex model of the QCM theory is given by the following equation.

$$\square_{\square,\square} = \sum_{\square=1}^{\square_{\square}} \sum_{\square=1}^{\square_{\square}} \sum_{\square=1}^{\square_{\square}} \square_{\square,\square\square\square}(\square_{\square})\square^{\square}_{\square,\square\square\square}\,\Delta\square_{\square,\square\square} + \sum_{\square=1}^{\square_{\square}} \sum_{\square=1}^{\square_{\square}} \sum_{\square=1}^{\square_{\square}-1} \square_{\square,\square\square}(\square_{\square-\square})\square^{\square}_{\square,\square\square\square} \tag{22}$$

Where

$$\Delta\square_{\square,\square\square} = \frac{\square\square(\square_{\square,\square})}{2\square_{\square}} \sin\frac{2\square-1}{\square_{\square}}\square$$

$$\square_{\square,\square\square}(\square_{\square}) = \sum_{\square=1}^{\square_{\square}} \square_{\square,\square\square\square}(\square_{\square})\Delta\square_{\square,\square\square}$$

$$\square_{\square,\square} = \sum_{\square=1}^{\square_{\square}} \sum_{\square=1}^{\square_{\square}} \square_{\square,\square\square}(\square_{\square})\square^{\square}_{\square,\square\square}\,\Delta\square_{\square,\square\square} + \sum_{\square=1}^{\square_{\square}} \sum_{\square=1}^{\square_{\square}-1} \square_{\square,\square\square}(\square_{\square-\square})\square^{\square}_{\square,\square\square} \tag{23}$$

Where

$$\Delta\square_{\square,\square\square} = \frac{\square\square_{\square}}{2\square_{\square}} \sin\frac{2\square-1}{\square_{\square}}\square$$

$$\square_{\square,\square}(\square_{\square}) = \sum_{\square=1}^{\square_{\square}} \square_{\square,\square\square}(\square_{\square})\Delta\square_{\square,\square\square}$$

In this way, the velocity vector $\square_{\square}$ around a propeller in the propeller coordinate systems and the velocity vector $\square_{\square}$ around a duct in the duct coordinate systems are expressed as

$$\square_{\square} = \square_{\square,\square} + \square_{\square\square,\square} + \square_{\square\square,\square} \tag{24}$$

$$\square_{\square} = \square_{\square,\square} + \square_{\square\square,\square} + \square_{\square\square,\square} \quad (25)$$

Where $\square_{\square,\square}$ and $\square_{\square,\square}$ are inflow vectors of propeller and duct respectively.
$\square_{\square\square,\square}$= induced velocity vector on the propeller due to the horseshoe vortex of the propeller.
$\square_{\square\square,\square}$ = induced velocity vector on the propeller due to the horseshoe vortex of the duct.
$\square_{\square\square,\square}$= induced velocity vector on the duct due to the horseshoe vortex of the propeller.
$\square_{\square\square,\square}$= induced velocity vector on the duct due to the horseshoe vortex of the duct.
The boundary conditions at the control points on the mean camber surfaces of propeller and duct are that there is no flow across the surfaces. Therefore the equation of the boundary condition is given as follow:

$$\square_{\square} \cdot \square_{\square} = \square \quad (26)$$

$$\square_{\square} \cdot \square_{\square} = \square \quad (27)$$

Where $\square_{\square}$ and $\square_{\square}$ is the normal vector on the mean camber surfaces of propeller and duct.

3.5 Calculation of Forces Acting on Propeller and Duct

Forces acting on the propeller blades and the duct can be expressed as

$$\square = \square_{\square} + \square_{\square} \quad (28)$$

The force $\square_{\square}$ acting on the bound vortex segments can be calculated by Kutta-Joukowski theorem as

$$\square_{\square} = \square\square \cdot \frac{\square}{\square\square}\left(\square^{\square}_{\square\square+} - \square^{\square}_{\square\square-}\right) \times \square_{\square} \quad (29)$$

Where

$$\square^{\square}_{\square\square+} - \square^{\square}_{\square\square-} = \frac{\square\square_{\square}}{2\square}\sum_{\square^{*}=1}^{\square}\square^{\square}_{\square\square^{*}}(\square)\sin\square_{\square}$$

where $\square$ is the fluid density and $\square_{\square}$ is the bound vortex segment. $\square_{\square}$ is the resultant velocity at the midpoint of a bound vortex segment. $\square_{\square}$ is the segment vector of the bound vortex segment. $\left(\square^{\square}_{\square\square+} - \square^{\square}_{\square\square-}\right)$ means the jump in tangential velocity across the camber surface and is equal to the strength of the vorticity $\square$.
The viscous drag $\square_{\square}$ can be expressed as

$$\square_{\square} = \frac{\square}{\square}\square\,\square_{\square}\square_{\square}|\square_{\square}||\square_{\square}| \quad (30)$$

The viscous drag coefficient $\square_{\square}$ is calculated empirically as (Nakamura, 1985).
The thrusts and torque acting on the propeller and duct are calculated by

$$\square = \sum_{\square=1}^{\square}\frac{\square\square_{\square}}{2\square_{\square}}\square_{\square\square}\sin\square_{\square} \quad (31)$$

$$\square = \sum_{\square=1}^{\square}\frac{\square\square_{\square}}{2\square_{\square}}(\square_{\square}\square_{\square\square} - \square_{\square}\square_{\square\square})\sin\square_{\square} \quad (32)$$

The thrust coefficients $\square_{\square,\square}$ and $\square_{\square,\square}$ of the propeller and the duct and the total thrust coefficient $\square_{\square}$ are defined by

$$\square_{\square,\square} = \frac{\square_{\square}}{\square\square^{2}\square_{\square}^{4}} \quad (33)$$

$$\square_{\square,\square} = \frac{\square_{\square}}{\square\square^{2}\square_{\square}^{4}} \quad (34)$$

$$\square_{\square} = \frac{\square_{\square} + \square_{\square}}{\square\square^{2}\square_{\square}^{4}} = \square_{\square,\square} + \square_{\square,\square} \quad (35)$$

Where $\square = \Omega/(2\pi)$ is the number of propeller rotation. Similarly, the torque coefficient $\square_{\square}$ and $\square$ of the propeller are defined by

$$\square_{\square} = \frac{\square}{\square\square^{2}\square_{\square}^{5}} \quad (36)$$

$$\square = \frac{\square\square_{\square}}{2\square\square_{\square}} \quad (37)$$

4 CALCULATION

The authors select highly skewed propeller (HSP) of Seiun-Maru-I in order to verify the present calculation compare the Hoshino's calculation results using panel method (Hoshino 1998a). Furthermore, the authors evaluated the propeller performance with various energy saving ducts in wake of Seiun-Maru-I to study on the mechanism of the energy saving ducts.
Table 1 shows the principal particulars and Table 2 shows the test condition. Distributions of loading points and the control points on the mean camber surfaces of the propeller are shown in Fig. 7. Camber surface is divided into 15 segments in the chordwise direction and 15 segments in the radial direction.
The time step $\square\square$ is given by the following equation.

$$\square\square = \square\square/360.0/\square$$

Where $\square\square$ is chosen as $\square\square$ = 10 degrees.
Calculations are performed using the Seiun-Maru's wake distribution (see Figure 8) given by the reference (Hoshino 1998b).

Table 1: Principal particulars of propellers (Seiun-Maru-I)

Name of Propeller	HSP
Diameter (m)	3.600
Number of Blade	5
Pitch Ratio at 0.7R	0.944
Expanded are Ratio	0.7
Hub Ratio	0.1972
Rake Angle (deg.)	-3.03
Blade Section	Modified SRI-B

Table 2: Test Condition

□, Ship Speed (knots)	9.0
□, Rotation Speed (rpm)	90.7
□ = □/□□	0.851

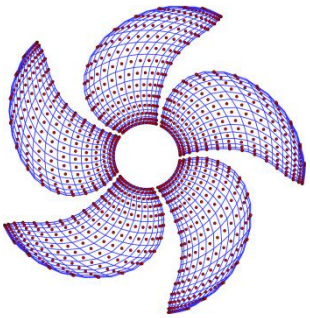

Figure 7: Distributions of the horseshoe vortices (blue lines) and the control points (red points) on the mean camber surfaces of the propeller.

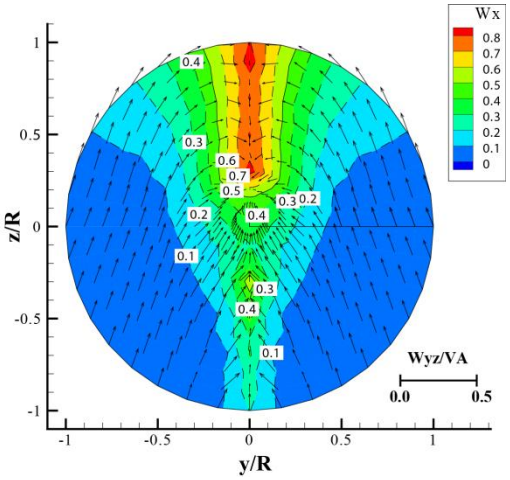

Figure 8: Wake velocity distribution of Seiun-Maru-I

4.1 Verification of Present Calculation on Propeller without Duct

Fig. 9 shows the calculated thrust and torque fluctuations acting on one blade of HSP comparing with the results of Hoshino's panel method (Hoshino, 1998b). It is found that the calculated results agree well with the Hoshino's results except for the angular position around Θ = 0 degree.

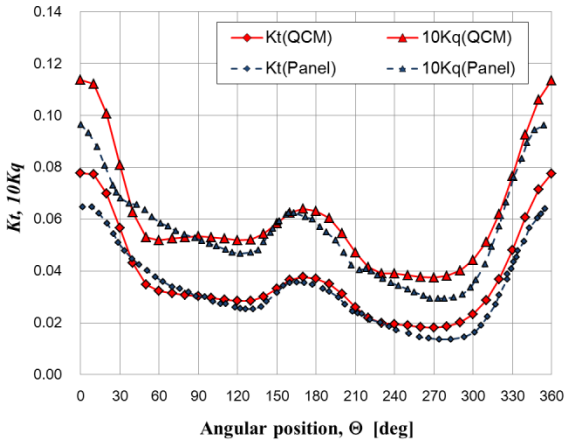

Figure 9: Comparison of thrust and torque coefficients fluctuation.

4.2 Study on Mechanism of Energy Saving Duct

In order to investigate the mechanism of energy saving ducts, the authors evaluated the propeller characteristics with the energy saving duct in uniform flow. Furthermore, 4 types of duct are evaluated in Seiun-Maru's wake. Table 3 shows the principal particulars of the energy saving ducts. Distributions of loading points and the control points on the mean camber surfaces of the duct are shown in Fig. 10. Camber surface is divided into 10 segments in the chordwise direction and 36 segments in the circumferential direction. The test condition and other treatments are the same in the case without duct described in 4.1.

Table 3: Principal particulars of Energy Saving Duct

Shape of a Cross Section	NACA3C10
Diameter : □□ (m)	0.9
Length : □□ (m)	1.0
Attack Angle : □□ (deg.)	Duct A : □□ = *0.0* Duct B : □□ = *−3.0* Duct C : □□ = *3.0* Duct D : □□ = *6.0*
Distance of Between Propeller and Duct (□□□)	1.5

(1) Calculation in Uniform Flow

In the uniform flow calculation, duct A is used for the energy saving ducts. Comparison of the circulation distribution on one blade in the radial direction between w/o duct and with Duct A is shown in Fig 11. Fig.12 is shown the induced velocity on propeller surface due to the duct. It is found that the duct increases the inflow velocity on the propeller surface. Fig.11 shows the circulation on the propeller at the back of the duct is reduced. Fig.15 (a) shows the thrust of the duct in the uniform flow. From Fig.15 (a), the duct generates a drag in the uniform flow. Therefore, Duct A has no advantage for the energy saving in the uniform flow.

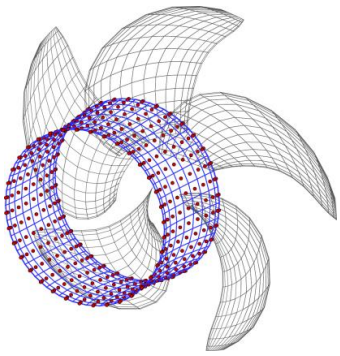

Figure 10: Distributions of the horseshoe vortices (blue lines) and the control points (red points) on the mean camber surfaces of Duct A.

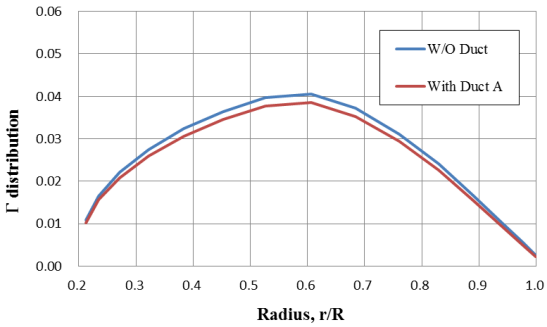

Figure 11: Comparison Γ distribution of the one blade in the uniform flow between w/o duct and w/ Duct A.

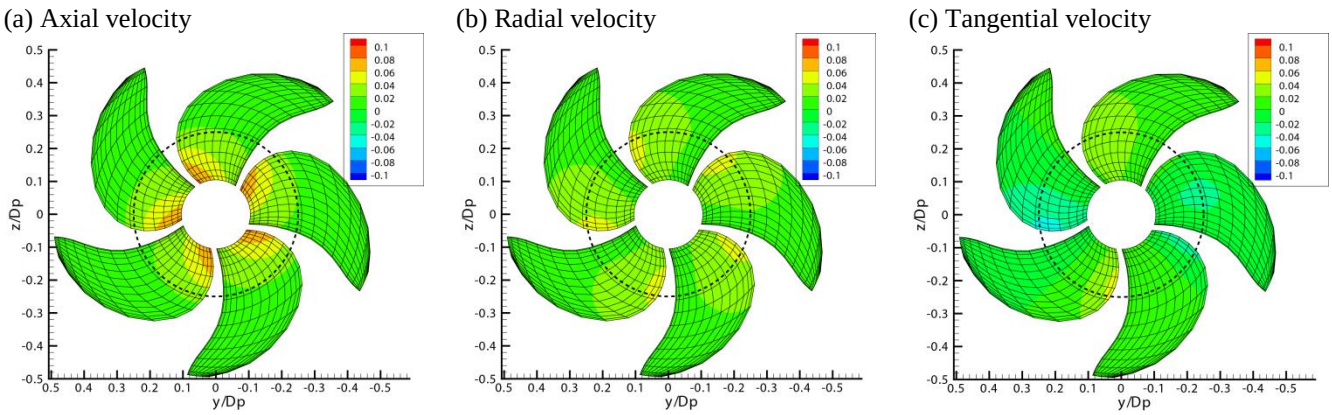

Figure 12: Comparison of induced velocity of propeller due to Duct A in the uniform flow.
Dashed circles show the position of leading edge of duct.

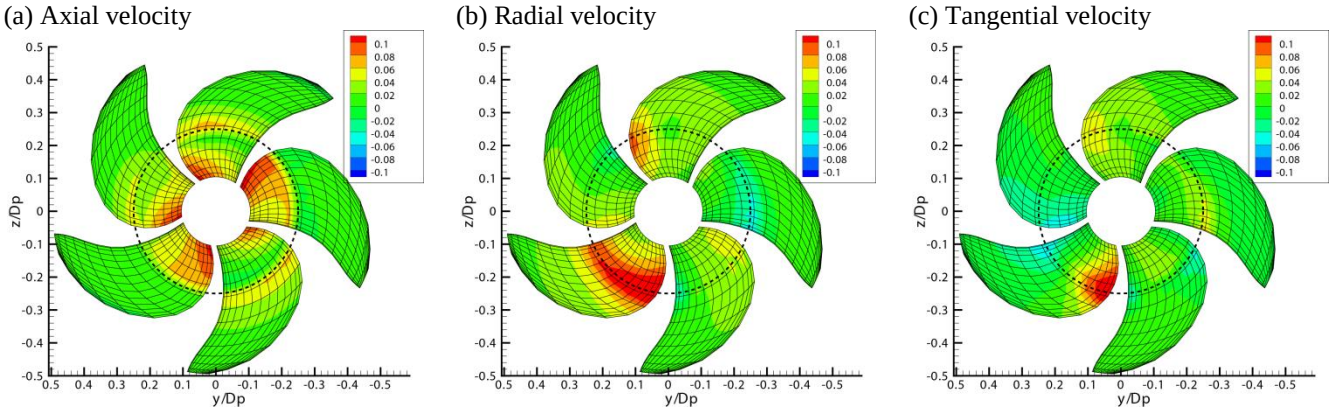

Figure 13: Comparison of induced velocity of propeller due to Duct A in the Seiun-Maru's wake.
Dashed circles show the position of leading edge of duct.

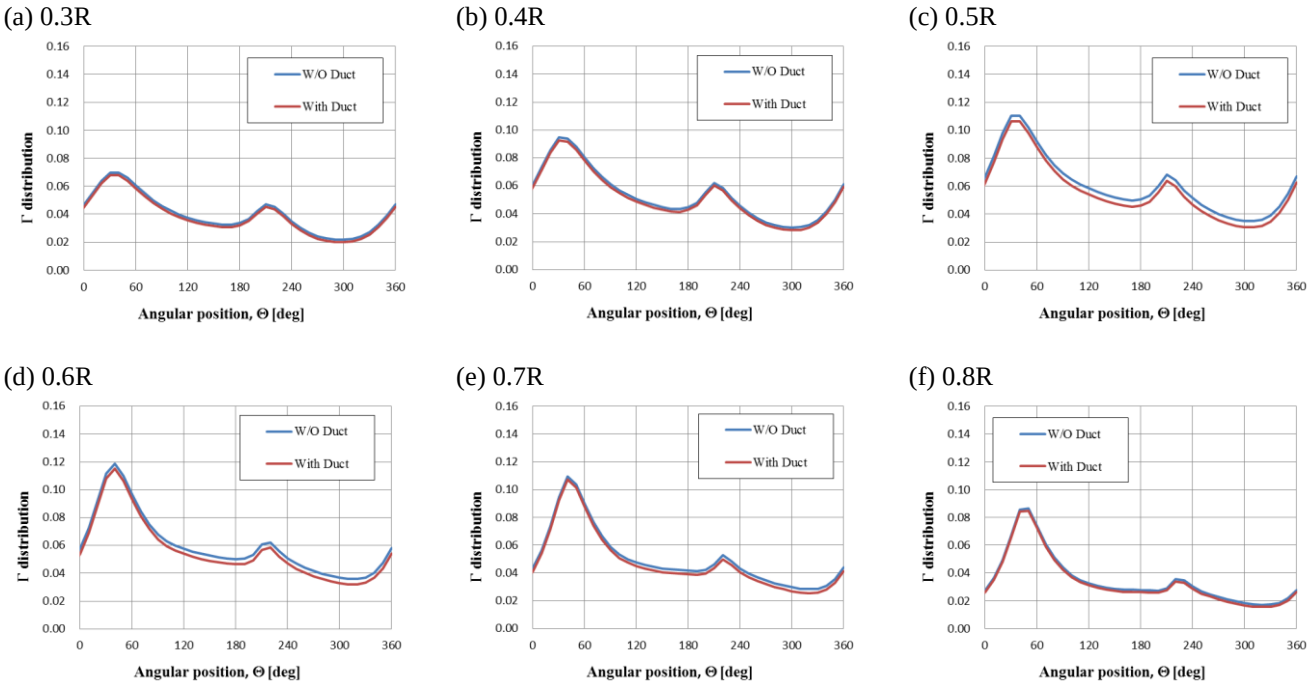

Figure 14: Comparison of Γ distribution on one blade in the Seiun-Maru's wake between w/o duct and w/ Duct A.

(a) Duct A in the uniform flow

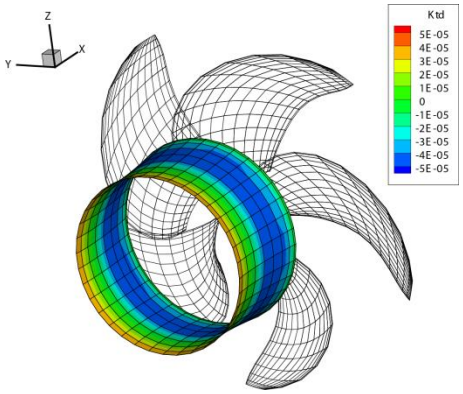

(b) Duct A in Seiun-Maru's wake

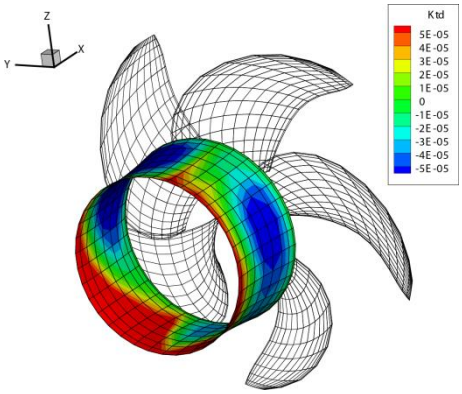

(c) Duct B degrees in Seiun-Maru's wake

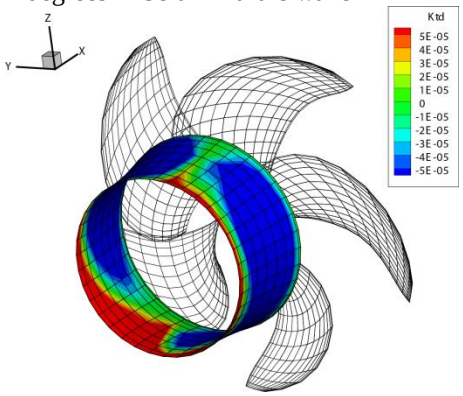

(d) Duct C in Seiun-Maru's wake

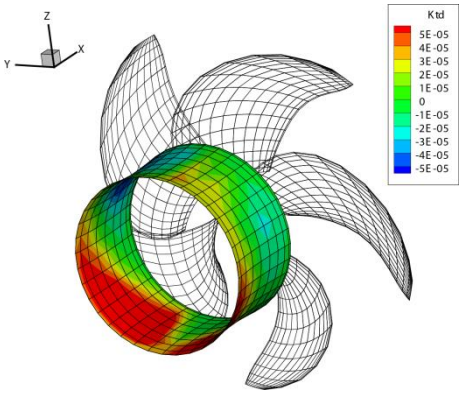

Figure 15: Thrust distribution of the various ducts in Seiun-Maru's wake (Propeller angular position is 0 degree.).

(a) Duct's thrust coefficient

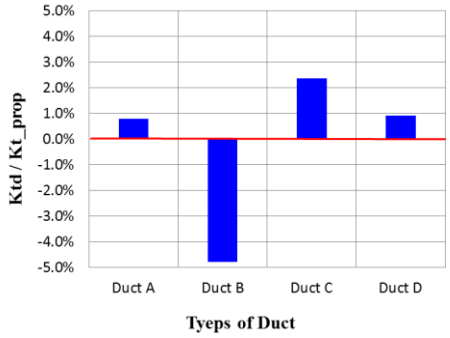

(b) Total thrust coefficient

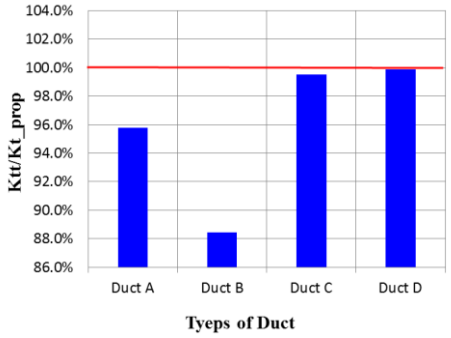

(c) Torque coefficient

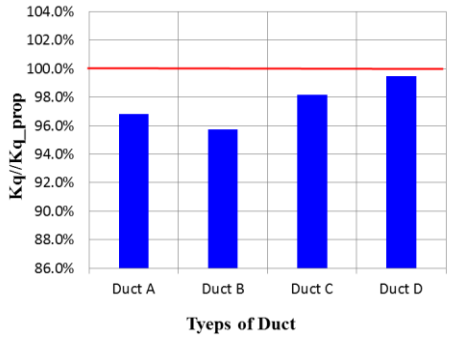

(d) Efficiency

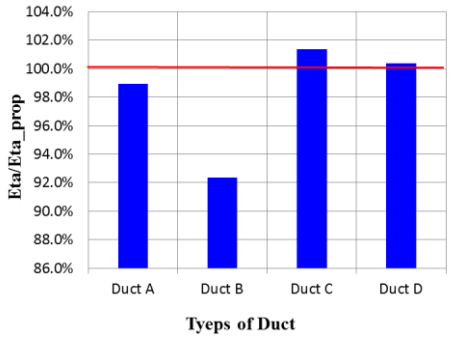

Figure 16: Comparison propeller characteristics in terms of the attack angle of duct.

(2) Calculation in Seiun-Maru's Wake

In the ship's wake, the propeller characteristics with 4 types of ducts are evaluated. The difference of these ducts is the attack angle of the duct's cross-section. The detail of these ducts is shown in Table 3. Fig.13 is shown the induced velocity on propeller surface due to the Duct A in the ship's wake. In the ship's flow, the inflow velocity on the propeller surface is increased in common with the case of uniform flow. Comparison of the circulation distribution at 0.3R – 0.8R sections during on revolution between w/o duct and with Duct A is shown in Fig 14. The circulation on the propeller at the back of the duct is reduced. This phenomenon in the ship's wake is similar to in the uniform flow. Comparison of propeller characteristics among these ducts in the ship's wake is shown in Fig.16. In this figure, ssubscripts "_prop" means propeller characteristics in the case of propeller w/o duct. All of ducts decrease the torque coefficient, because the duct increases the inflow to the propeller. In the lower part of Duct C, it generates strong lift force caused by the upstream of the ship's wake. Therefore, the efficiency of propeller with Duct C is the highest among these ducts. On the other hand, Duct B generates strong drag force. It causes the decease of the propeller efficiency.

5 CONCLUSIONS AND FUTURE WORK

In this paper, the authors presented the calculation method based on QCM for characteristics of propeller with energy saving duct in steady ship's wake. Comparison between the calculated results w/o and w/ the duct led the following conclusions:

(1) The present method can estimate of the effect of the energy saving duct.
(2) The ducts increase the inflow velocity on the propeller surface so that the propeller's circulation is decreased. It causes the decrease the thrust and torque of propeller.
(3) By adjustment the attack angle of duct's cross-section along downstream and upstream of ship's wake, the duct can generate the thrust effectively.
(4) It was found that the present method can be used for design tool of optimum propeller and duct.

As the future work, experimental measurement will be conducted to obtain the characteristics of propeller with some energy saving ducts. Then, the experimental data will be compared with the calculations of the present method in order to evaluate the accuracy. The calculated results will be analyzed and compared with the experimental data in order to discuss the applicability of the method as the design tool of marine propellers.

REFERENCES

Hanaoka, A., Kawanami, Y., and Hinatsu, M. (2014). "Application of Quasi-Continuous Method to Open-Water Characteristics Predictions of Propellers with Energy Saving Ducts," Proceedings 24th International Ocean and Polar Engineering Conference, Busan, pp 774-781.

Hanaoka, T. (1969). "Numerical Lifting-Surface Theory of a Screw Propeller in Non-Uniform Flow: Part 1 Fundamental Theory", Report of Ship Research Institute, Vol.5, No.5, pp.112-234.

Hoshino, T. (1985). "Application of Quasi-Continuous Method to Unsteady Propeller Lifting-Surface Problems," Journal of the Society of Naval Architects of Japan, Vol. 158, pp 48-68.

Hoshino, T. (1998a). "Comparative Calculations of Propeller Performance in Steady and Unsteady Flows Using a Surface Panel Method," 22nd ITTC Propulsion Committee Propeller RANS/Panel Method Workshop, Grenoble, France, April 1998, pp 327-342.

Hoshino, T. (1998b). "Experimental Data for Unsteady Panel Calculations and Comparisons (SEIUN-MARU HSP)," 22nd ITTC Propulsion Committee Propeller RANS/Panel Method Workshop, Grenoble, France, April 1998, pp 111-140.

Kanemaru, T. and Ando, J. (2009). "Numerical Analysis of Steady and Unsteady Sheet Cavitation on a Marine Propeller Using a Simple Surface Panel Method "SQCM"," Conference proceedings of First International Symposium on Marine Propulsors smp'09, Trondheim, Norway, Vol.6, pp 205-208.

Kawashima, H., Kume, K. and Sakamoto, N. (2014). "Study of Weather Adapted Duct (WAD)," Papers of National Maritime Research Institute, Vol.14, No.2, pp 19-34.

Koyama, K. (1975). "A Numerical Method for Propeller Lifting Surface in Non-Uniform Flow and Its Application," Journal of the Society of Naval Architects of Japan, Vol.137, pp.78-87.

Lan, CE (1974). "A Quasi-Vortex-Lattice Method in Thin Wing Theory," Journal of Aircraft, Vol. 11 No 9, pp 518-527.

Nakamura, N (1985). "Estimation of Propeller Open-Water Characteristics Based on Quasi-Continuous Method," Journal of the Society of Naval Architects of Japan, Vol. 157, pp 95-107.

Yuasa, H (1980). "Application of Numerical Lifting-Surface Theory on Steady Performance of Propeller / Duct System," Journal of the Society of Naval Architects of Japan, Vol.147, pp 53-61.

DISCUSSION

Question from Tom van Terwisga

Can you say something on the comparison of the duct effectiveness before open water condition and the condition behind the Seiun-maru?

Authors' Closure

Thank you for your insightful comment. We haven't compared the duct effectiveness before open water condition and the condition behind the wake. However, the effect of the duct in uniform flow has been examined. In the uniform flow, the duct generates drag and increases the flow inside of itself. It causes the decease of the propeller efficiency.

We agree that additional calculation as you suggested would be valuable. As the future work, the comparison calculation will be conducted.